Transactions of the Materials Research Society of Japan 32[4] 891-894 (2007)

Crystal Growth and Ferroelectric Properties of $BaTiO_3$ Thin Films Deposited on Si Substrate by Low Energy Ion Beam Assisted Deposition Technique

Yasuki Yamamoto, Yuuji Morigo and Katsuhiro Yokota
Faculty of Engineering and HRC, Kansai University, 3-3-35 Yamate-cho, Suita, Osaka 565-8680, Japan
Fax: 81-6-6388-8843, e-mail: kyokota@ipcku.kansai-u.ac.jp

$BaTiO_3$ thin films were deposited on silicon substrates by ionizing oxygen gas in evaporating Ti metals and $BaCO_3$ compounds. $BaTiO_3$ films were deposited after very thin films of TiN were deposited on Si substrates to prevent the oxidation of Si surfaces. The deposited $BaTiO_3$ thin films had tetragonal (t-) polycrystals oriented to the (101) crystalline plane. A $BaTiO_3$ film deposited using oxygen ion beams with an energy of 100 eV and a current of 0.16 mA/cm^2 had a large saturated polarization value of 39 μC/cm^2 and a polarization-electric field (*P-E*) hysteresis loop with a remanent polarization of 7.3 μC/cm^2 and a coercive field of 102.9 kV/cm. Their remanent polarization values decreased when the energies of oxygen ion beams were increased and decreased from 100 eV.
Key words: $BaTiO_3$, thin film, IBAD, *P-E* hysteresis loop, dielectric constant

1. INTRODUCTION

Ferroelectric thin films have received much attention due to their potential applications to novel devices. Barium titanate ($BaTiO_3$ or BTO) is one of the most remarkable ferroelectric materials which has a perovskite structure and possesses large dielectric constants and high resistivities [1-3]. $BaTiO_3$ crystals and ceramics promise applications of many devices such as FeRAM, multilayer capacitors and infrared detectors. Conventionally, thin $BaTiO_3$ films were deposited on templates such as Pt/Ti, Ti/Si, SiO_2/Si, Pt/SiO_2/Si and Pt/MgO/Si by reactive evaporation [4], metal organic chemical vapor deposition [5], rf-sputtering [6], sol-gel method [7] and laser ablation method [8]. The deposited films are commonly post-annealed in order to stabilize and crystallize at temperature higher than working temperature on device fabrication processes. Film cracking and hillocks are formed from bottom Pt electrodes during rapid cooling [9]. Assisting crystal growth with energetic ion beams is effective for lowering its crystallization temperature [10]. However, in depositing $BaTiO_3$ films on silicon (Si) substrates by an ion beam assisted deposition (IBAD) method, a thin SiO_2 layer is grown on the Si surface near the interface between the $BaTiO_3$ film and the Si substrate, and $BaTiO_3$ films deposited on Si substrates had degraded dielectric properties [11]. We considered employing TiN to prevent the formation of SiO_2 layers due to the diffusion of oxygen into Si substrates and in order to avoid the nasty problem relating to the bottom Pt electrode on conventional ferroelectric memory structures.

2. EXPERIMENTAL PROCEDURE

An IBAD system employed in this experiment is composed of two electron beam evaporators for evaporating Ti metals and $BaCO_3$ compounds, and an electron cyclotron resonance (ECR) ion source for ionizing O_2 and N_2 gas. Boron-doped (100) Si wafers with a resistivity of 0.5 ~ 1.0 Ω·cm were used as a substrate. The Si substrates were successively rinsed in solvent naphtha, acetone and methanol, and then loaded into the IBAD apparatus immediately after thin native oxide layers were removed in a 5% HF solution. First, a TiN thin film with a thickness of about 30 nm were deposited on Si substrates at temperature of 800°C by flowing N_2 gas with a rate of 30 sccm. The energy and current of N_2 ion beams were adjusted to 100 eV and 0.08 mA/cm^2, respectively. Then, $BaTiO_3$ films were deposited on the TiN/Si templates at a temperature of 800°C by flowing O_2 gas with a rate of 30 sccm. The evaporation rates of Ti metals and $BaCO_3$ compounds were 0.01 and 0.02 [nm/s], respectively. The energies of oxygen ion beams were adjusted in the range of 50 - 300 eV, and currents in the range of 0.16 - 0.31 mA/cm^2. The thickness of the deposited $BaTiO_3$ films was measured by using a laser confocal microscope and was about 200 nm.

The structural characteristic of the $BaTiO_3$ thin films was analyzed by X-ray diffraction (XRD) with Cu *Kα* radiations in Seeman-Bohlin geometry (λ ~ 0.154 nm) operating at the θ-2θ scanning mode and the incident angle of 1°. The measured peaks were assigned to known crystal lattice planes by using a powder diffraction file [13]. Aluminum was evaporated on surfaces of $BaTiO_3$ films and back-faces of Si substrates. The Al electrodes on the Si back-face were alloyed at a temperature of 300°C in argon atmosphere for 10 min. Polarization-electric field (*P-E*) hysteresis loops of $BaTiO_3$ films were measured by using a Sawyer-Tower circuit with a sinusoidal sweeping voltage at a frequency of 10 kHz [14].

3. RESULTS AND DISCUSSION

3.1 Crystalline structures

Figure 1 shows XRD patterns of barium-titanium-oxygen compound (Ba-Ti-O) films deposited using oxygen ion beams with an energies of 50 - 300 eV with a current of 0.16 mA/cm^2 at a temperature of 800°C. The deposited $BaTiO_3$ films consisted of tetragonal (t-) crystallites oriented preferentially to the (101) crystal planes. The $BaTiO_3$ films oriented preferentially to (110) crystal plane were deposited using conventional methods not employing oxygen ion beams [4-8]. In this experiment, the preferentially (101) oriented $BaTiO_3$ films were deposited using oxygen ion beams. Ba_2TiO_4, $BaTi_2O_5$, and

$BaTiO_3$ crystallites grew in Ba-Ti-O films deposited by applying oxygen ion beams with an energy of 50 eV. The Ba_2TiO_4 and $BaTi_2O_5$ crystallites did not grow in Ba-Ti-O films deposited using oxygen ion beams with energies larger than 50 eV, but $BaTiO_3$ crystallites only grew. The XRD angles (2θ) for $BaTiO_3$ crystallites on the 100 eV-deposited films were well corresponding to those in the powder diffraction file [13]. Here, for example, the 100 eV deposited film shows a Ba-Ti-O film deposited using an oxygen ion beams with an energy of 100 eV. They were larger than those on the 50 eV- and 300 eV-deposited films and were approximately the same as those on the 200 eV deposited film. On the other hand, the 2θ values of the (111) and (112) XRD peaks were the same on $BaTiO_3$ films deposited with oxygen ion beams with energies lower than 200 eV while the 300 eV deposited $BaTiO_3$ film had the (111) and (112) XRD peaks measured at 2θ values slightly smaller than those deposited with low energy oxygen ion beams.

Oxygen ions of $1x10^{15}$ ions/cm^2/s, corresponding to 0.16 mA/cm^2, hit the surfaces of $BaTiO_3$ films during deposition while O_2 molecules of $1.3x10^{19}$ molecules/cm^2/s, corresponding to 30 sccm, are carried onto the film surfaces. The oxygen ion beams remove only small amounts of Ba atoms, Ti atoms and O atoms from $BaTiO_3$ films because of their sputtering yields smaller than one [12]. Oxygen lost lattice sites are filled immediately because a great amount of O_2 molecules are carried out on the surfaces of Ba-Ti-O films. Loss of Ba atoms from $BaTiO_3$ films is more than that of Ti atoms and increases with increasing oxygen ion beam energy [12]. The XRD peaks will be measured at positions larger than the original 2θ values in a powder diffraction file [13], although the 300 eV deposited $BaTiO_3$ film had XRD peaks at positions smaller than the original 2θ values.

50 eV deposited Ba-Ti-O films had compounds such as Ba_2TiO_4, $BaTi_2O_5$ other than $BaTiO_3$ because the ion beam energy is very close to the threshold energy for sputtering compounds, and because excess O_2 molecules were carried on the film surface. However, $BaTiO_3$ films were deposited with oxygen ion beams with an energy of 100 eV. Energetic oxygen ions can assist the growth of $BaTiO_3$ by releasing their kinetic energy on the depositing film surfaces because migrations of constituents on film surfaces are enhanced by the energetic oxygen ions [10]. If the surface migration of constituents is insufficient for the occupancy of constituents onto regular lattice sites, some of constituents are captured on boundaries between crystallites and are present as interstitial atoms in the crystalline unit cell. The interstitial atoms serve to extend the crystalline lattices. The XRD peaks on crystals with interstitial atoms are observed at the position of 2θ smaller than the original 2θ. With increasing oxygen ion beam energy, many vacant lattice sites are developed in crystals, and many O atoms are implanted into the crystalline unit cell [12]. If the loss of atoms in the unit cell by sputtering is larger than the amount of interstitial atoms by ion-implantation, the XRD peaks on the deposited film are measured at 2θ values larger than the original 2θ values because vacant lattice sites are developed and the unit cells become smaller. Thus, the shifts of the XRD peaks toward small 2θ values seem to occur because the 300 eV deposited Ba-Ti-O film had the number of implanted

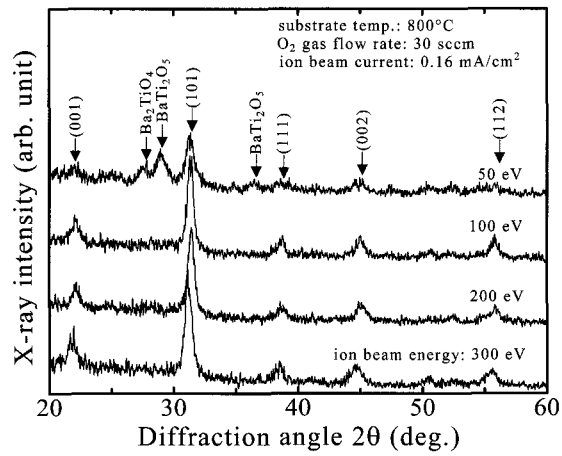

Fig. 1. XRD patterns of deposited Ba-Ti-O films as a function of oxygen ion beam energy.

O atoms more than that of elements removed by sputtering, and because the 50 eV-deposited Ba-Ti-O film had small surface migrations of elements.

Figure 2 shows XRD patterns of Ba-Ti-O films deposited using oxygen ion beams with currents of 0.16 - 0.31 mA/cm^2 and an ion beam energy of 100 eV at a temperature of 800°C. Large XRD peaks from t-$BaTiO_3$ crystallites and very small XRD peaks from $BaTi_2O_5$ crystallites were observed on films deposited with ion beam currents of 0.24 and 0.31 mA/cm^2. However, a 0.16 mA/cm^2-deposited Ba-Ti-O film had only XRD peaks from t-$BaTiO_3$ crystallites. The intensity of the (101) XRD peak became maximum on the 0.16 mA/cm^2-deposited Ba-Ti-O film. Here, XRD spectra on Ba-Ti-O films deposited with oxygen ion beam currents smaller than 0.16 mA/cm^2 were not given because those like to those on Ba-Ti-O films deposited with larger oxygen ion beam currents. A small number of energetic oxygen ions results in a small number of constituents with surface migration accelerated by energetic ion collision [10]. However, a large number of energetic oxygen ions result in a large number of interstitial atoms because the number of oxygen ions implanted into $BaTiO_3$ unit cells is proportional to that of energetic oxygen ions. Thus, a large number of t-$BaTiO_3$ crystallites were contained in a Ba-Ti-O film deposited with an ion beam energy of 100 eV and a ion beam current of 0.16 mA/cm^2.

3.2 *P-E* hysteresis loops and ferroelectric properties

Figure 3 (a) and (b) show *P-E* hysteresis loops of Ba-Ti-O films deposited using oxygen ion beams with energies of 50 - 300 eV and a current of 0.16 mA/cm^2 at a temperature of 800°C. The *P-E* hysteresis loops were largely improved in comparison with those for $BaTiO_3$ films deposited directly on Si substrates [11]. The shapes of the *P-E* hysterisis loops were slim and showed incomplete saturation. The similar *P-E* hysteresis loops has been reported for $BaTiO_3$ films consisting of nonferroelectric layers [15], Pb(Zr, Ti)O_3 films [16, 17] and $BiScO_3$ films [18]. The polarization value of 100 eV-deposited Ba-Ti-O film was maximum in this experiment because the film consisted of $BaTiO_3$ crystallites with the lattice constants given in a powder

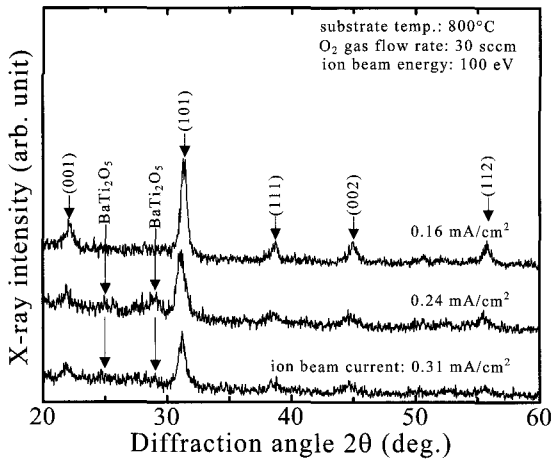

Fig. 2. XRD patterns of deposited films as a function of oxygen ion beam current.

diffraction file [13]. However, other Ba-Ti-O films consisted of $BaTiO_3$ crystallites with extended unit cells because of presence of interstitial atoms due to ion-implantation, as described already. The interstitial atoms hinder a displacement of ions in the $BaTiO_3$ unit cell by applying electric field. The polarization value of the 100 eV-deposited Ba-Ti-O film had a saturated value of 39 $\mu C/cm^2$ had the unit cell with the volume of about 6.45×10^{-23} cm^3. That is, the dipole moment of the cell is calculated to be 2.5×10^{-27} C·cm. If the positive ions of Ba^{2+} and Ti^{4+} are moved by δ with respect to the negative ions of O^{2-}, the dipole moment of the cell can be calculated as $6q\delta$, where q is the electric charge. The displacement δ is estimated to be about 0.026 nm on the $BaTiO_3$ film and about ten times as large as those of $BaTiO_3$ films deposited with oxygen ion beams with energy of 50, 200 and 300 eV. The displacement of 0.026 nm is approximately the same as that in bulk t-$BaTiO_3$ [19]. The small displacements of positive ions such as Ba^{2+} and Ti^{4+} on the 50, 200 and 300 eV-deposited films seem that the displacements of ions in the unit cell by electric field were hindered by interstitial atoms.

Figure 4 shows dielectric constants as a function of oxygen ion beam energy. The maximum dielectric

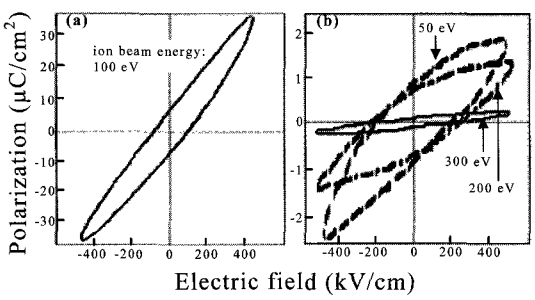

Fig. 3. P-E hysteresis loops at room temperature. 0.16 mA/cm^2-deposited Ba-T-iO films under an O_2 gas flow rate of 30 sccm at a substrate temperature of 800°C. (a) for a film deposited at an energy of 100 eV, (b) for a films deposited with energies of 50, 200 and 300 eV.

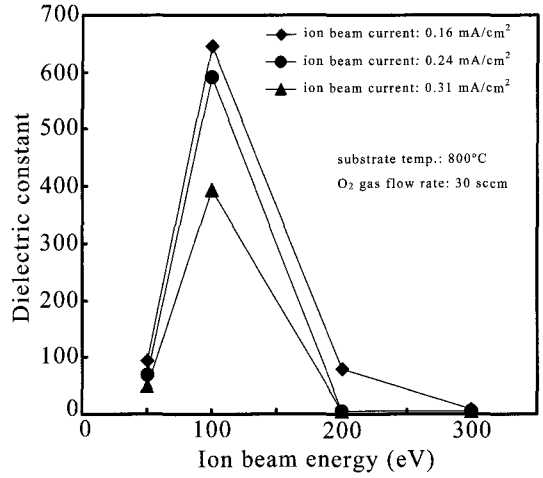

Fig. 4. Ion beam energy dependence of dielectric constant for Ba-Ti-O films deposited with oxygen ion beam currents of 0.16 - 0.31 mA/cm^2.

constant of $645.4\varepsilon_0$ was measured the 100 eV-deposited Ba-Ti-O films at an ion beam current of 0.16 mA/cm^2, where ε_0 is the dielectric constant in vacuum. The obtained dielectric constant was larger than those of conventional $BaTiO_3$ thin films and smaller than bulks [20].

Figures 5 and 6 show values of remanent polarization and coercive field were plotted as a function of oxygen ion beam energy. The remanent polarization values increased with increasing oxygen ion beam energy and then decreased after reached a maximum value at 100 eV. On the other hand, the coercive field value depended on oxygen ion beam energy in opposition to that of the remanent polarization values and became the minimum on the 100 eV-deposited Ba-Ti-O films. An increase in oxygen ion beam current resulted in the degradation of remanent polarization and coercive field values because the number of radiation damages, containing vacancies, displacement atoms and implanted

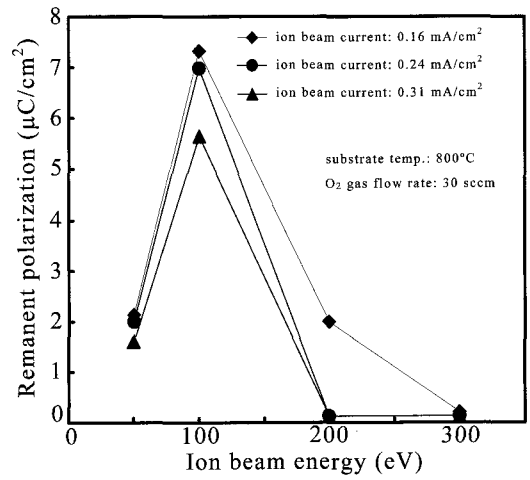

Fig. 5. Ion beam energy dependence of remanent polarization for Ba-Ti-O films deposited with oxygen ion beam currents of 0.16 - 0.31 mA/cm^2.

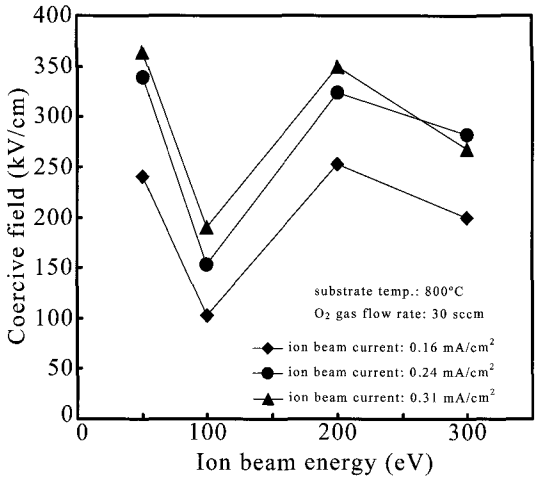

Fig. 6. Ion beam energy dependence of coercive field for Ba-Ti-O films deposited with oxygen ion beam currents of 0.16 - 0.31 mA/cm^2.

containing vacancies, displacement atoms and implanted atoms by applying oxygen ion beams, increases with increasing oxygen ion beam current. A 100 eV-deposited Ba-Ti-O film only had approximately the same lattice constants as conventional $BaTiO_3$ crystals [13]. Other films had extended crystalline lattices because interstitial atoms are generated by oxygen ion implantation during deposition. The displacements of ions in unit cells by applying electric field become larger on the 100 eV-deposited Ba-Ti-O film and smaller on other films with interstitial atoms more than the 100 eV-deposited Ba-Ti-O film. Electric currents in deficient dielectric films can be represented by the Poole-Frenkel mechanism [21]. The Poole-Frenkel currents were measured on deposited Ba-Ti-O films although the results were not shown here.

4. CONCLUSION

Tetragonal-$BaTiO_3$ films were deposited on Si substrates by an IBAD technique after the deposition of thin TiN films. Ba-Ti-O films consisted of many $BaTiO_3$ crystallites oriented preferentially to the (101) crystal planes, and Ba-Ti-O films other than the 100 eV-deposited film consisted of crystallites with extended lattices. The dielectric properties of the $BaTiO_3$ films strongly depended on oxygen ion beam energy the surface migrations of constituents are enhanced by application of oxygen ion beams, and because interstitial atoms are generated in crystalline lattices by ion-implantation. A suitable dielectric property was realized on the 100 eV-deposited films: they had approximately the same lattice constants as the standard $BaTiO_3$ crystallite, a large remanent polarization of 7.3 $\mu C/cm^2$ and a small coercive field of 102.9 kV/cm.

REFERENCES

[1] K. Abe, N. Yanase and T. Kawakubo, Jpn. J. Appl. Phys., Part 1 **40**, 2367 (2001).
[2] Yu. A. Boikov and T. Claeson, J. Appl. Phys., **89**, 5053 (2001).
[3] R. Waser, Nanoelectronics and Information Technology, Wiley-VCH, Weinheim, 2003.
[4] T. Kuroiwa, Y. Tsunemine, T. Horikawa, T. Makita, J. Tanimura, N. Mikami and K. Sato, Jpn. J. Appl. Phys., **33**, 5187 (1994).
[5] Z. Wang, T. Yasuda, S. Hatatani and S. Oda, Jpn. J. Appl. Phys., **38**, 6817 (1999).
[6] K. Ijima, T. Terashima, Y. Bando, K. Kamigaki and H. Terauchi, J. Appl. Phys., **72**, 2840 (1992).
[7] T. Hayashi and T. Tanaka, Jpn. J. Appl, Phys., **34**, 5100 (1995).
[8] B. D. Qu, M. Evstigneev, D. J. Johson and R. H. Prince, Appl, Phys. Lett., **72**, 1394 (1998).
[9] O. Auciello and J. Engemann, Multicomponent and Multilayerd Thin Films for Advanced Microtechnologies, Techniques, Fundamentals and Devices, Kluwer Academic, Doredrecht, 1993, NATO/ASI Book Series E, **243** p.116.
[10] T. Yoshimi: Plasma CVD Technology, in K. Hozumi ed., Plasma Chemistry, Kogyo-chousakai, Tokyo, 1983, p.105-119.
[11] K. Yokota, A. Takeda, Y. Kawasaki and K. Nakamura, Jpn. J. Appl. Phys., **44**, 8544-8546 (2005).
[12] J. F. Ziegler and J. P. Biersach, The Stopping and Range of Ions in Matter (http://www.srim.org /SRIM/SRIMLEGL.htm, 2003).
[13] Joint Committee for Powder Diffraction Standards, Powder Diffraction File, Int. Center for Diffraction Data, Park Lane, No. 5-626, 34-133 and 35-813, 1989.
[14] N. Ashkenov, M. Schubert, E. Twerdowski, H. V. Wenckstern, B. N. Mbenkum, H. Hochmuth, M. Lorenz, W. Grill and M. Grundmann, Thin Solid Films, **486**, 153-157 (2005).
[15] Z. Wei, M. Noda and M. Okuyama, Jpn. J. Appl. Phys., **41**, 6619 (2002).
[16] P. J. Schom, D. Brauhaus, U. Bottger, R. Waser, G. Beite, N. Nagel and R. Bruchhaus, J. Appl. Phys, **99**, 114104 (2006).
[17] J. S. Cross, K. Kurihara, I. Sakaguchi and H. Haneda, J. Appl. Phys, **99**, 124105 (2006).
[18] H. Wen, X. Wang, X. Deng and L. Li, Appl. Phys. Lett., **88**, 222904 (2006).
[19]C. Kittel, Introduction to Solid State Physics, 8th ed., Wiley, Danvers, 2005, p.471.
[20] Z. Wei, M. Noda and M. Okuyama, Jpn. J. Appl. Phys., **41**, 6691 (2002).
[21] S. M. Sze, Physics of Semiconductor Devices, 2nd ed., Wiley, New York, 1981, chap.7.

(Received December 10, 2006;Accepted May 15, 2007)